nature astronomy

Review article

https://doi.org/10.1038/s41550-024-02339-z

High-energy neutrinos from the vicinity of the supermassive black hole in NGC 1068

Received: 1 December 2023

Accepted: 15 July 2024

Published online: 18 September 2024

Check for updates

P. Padovani[1] ✉, E. Resconi[2], M. Ajello[3], C. Bellenghi[2], S. Bianchi[4], P. Blasi[5,6], K.-Y. Huang[7], S. Gabici[8], V. Gámez Rosas[9], H. Niederhausen[10], E. Peretti[8,11], B. Eichmann[12], D. Guetta[13], A. Lamastra[14] & T. Shimizu[15]

We present a comprehensive multi-messenger study of NGC 1068, the prototype Seyfert II galaxy associated with high-energy neutrinos following a detection by the IceCube Neutrino Observatory. Various aspects of the source, including its nuclear activity, jet, outflow and starburst region, are analysed in detail using a multi-wavelength approach and relevant luminosities are derived. We then explore its γ-ray and neutrino emissions and investigate the potential mechanisms underlying these phenomena and their relations with the different astrophysical components to try to understand which is responsible for the IceCube neutrinos. By first using simple order-of-magnitude arguments and then applying specific theoretical models, we infer that only the region close to the accretion disk around the supermassive black hole has the right density of both the X-ray photons needed to provide the targets for protons to sustain neutrino production and the optical/infrared photons required to absorb the associated, but unobserved, γ-rays. We conclude by highlighting ongoing efforts to constrain a possible broad connection between neutrinos and active galactic nuclei, as well as future synergies between astronomical and neutrino facilities.

Eleven years ago the IceCube Neutrino Observatory (http://icecube.wisc.edu) reported for the first time the detection of high-energy astrophysical neutrinos of likely extragalactic origin with energies in the teraelectronvolt–petaelectronvolt range (10^{12}–10^{15} eV)[1,2]. This detection implies the existence of a class of astrophysical objects accelerating protons up to at least 10–100 PeV, which then collide with other protons (p–p collisions) or photons (p–γ collisions). So far, however, searches performed by the IceCube collaboration have associated only the Galactic Plane[3] and two extragalactic objects with neutrinos at a significance greater than ~3σ. These are the blazar TXS 0506+056 at redshift $z = 0.3365$ (at the 3–3.5σ level)[4,5] and the prototype local Seyfert II galaxy NGC 1068 (ref. 6). The latter study reported 4.2σ evidence for an excess of teraelectronvolt neutrinos from the direction of this source. As shown in Fig. 1, however, the 68% confidence region around the most significant neutrino spot embeds the whole galaxy. Hence the resolution of the IceCube detector does not allow us to identify the region responsible for the cosmic ray acceleration and neutrino production processes, leaving the origin of these neutrinos an open question.

[1]European Southern Observatory, Garching, Germany. [2]Department of Physics, TUM School of Natural Sciences, Technical University of Munich, Garching, Germany. [3]Department of Physics and Astronomy, Clemson University, Clemson, SC, USA. [4]Dipartimento di Matematica e Fisica, Università degli Studi Roma Tre, Rome, Italy. [5]Gran Sasso Science Institute, L'Aquila, Italy. [6]INFN–Laboratori Nazionali del Gran Sasso, Assergi, Italy. [7]Leiden Observatory, Leiden University, Leiden, the Netherlands. [8]Astroparticule et Cosmologie, Université Paris Cité, CNRS, Paris, France. [9]Sterrewacht Leiden, Leiden, the Netherlands. [10]Department of Physics and Astronomy, Michigan State University, East Lansing, MI, USA. [11]Niels Bohr International Academy, Niels Bohr Institute, University of Copenhagen, Copenhagen, Denmark. [12]Theoretische Physik IV, Fakultät für Physik und Astronomie, Ruhr-Universität Bochum, Bochum, Germany. [13]Physics Department, Ariel University, Ariel, Israel. [14]INAF–Osservatorio Astronomico di Roma, Rome, Italy. [15]Max-Planck für extraterrestrische Physik, Garching, Germany. ✉e-mail: ppadovan@eso.org

https://doi.org/10.1038/s41550-024-02339-z

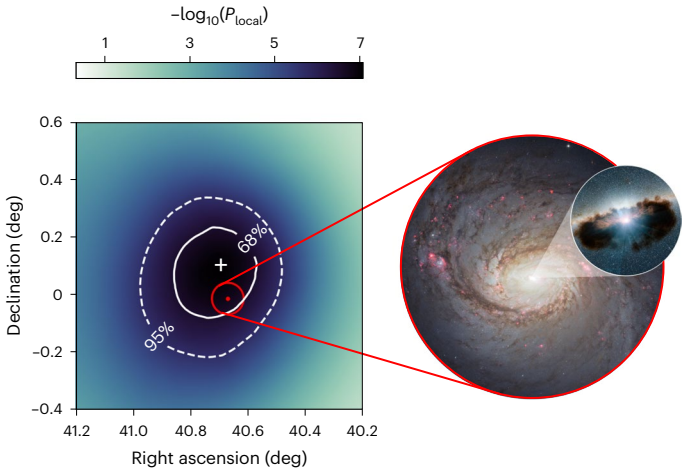

Fig. 1 | Significance map around the location of NGC 1068. Left: significance map, where $P_{\rm local}$ is the local p-value. The white cross indicates the most significant location in the neutrino sky and the white solid (dashed) contours show the 68% (95%) confidence regions around it. The red dot and the circle around it indicate the position and optical size of NGC 1068. Right: an image of the spiral galaxy and an illustration of its active nucleus surrounded by the dusty torus (inset). Panels adapted with permission from: left, ref. 6, AAAS; right, NASA/JPL-Caltech.

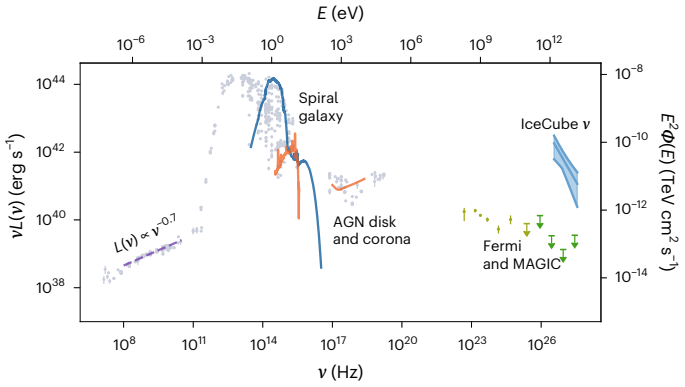

Fig. 2 | The integrated multi-messenger SED of NGC 1068. The SED shows the power emitted at different frequencies/energies with various components highlighted with coloured lines and symbols. Units are: frequency ν in Hz (bottom x axis), energy E in eV (top x axis), power L in erg s^{-1} (left y axis), and flux $E^2\,\Phi(E)$ in TeV cm^2 s^{-1} (right y axis). Error bars of Fermi data (khaki points) denote 68% uncertainties, while the MAGIC data (green points) represent 95% confidence level upper limits. Note that the SED tool provides multiple values at the same frequency that reflect the different resolutions used by the facilities that have studied the source on various spatial scales. For clarity we have kept mainly the highest flux values, which are associated with the largest scales, as the SED is dominated by the host galaxy given its relatively small distance. Figure created with SED Builder, SSDC (https://tools.ssdc.asi.it/SED).

The main motivation of this Review is to discuss the relevant astrophysical components of NGC 1068, understand their nature and constrain the origin of its neutrino emission from an observational, phenomenological and theoretical multi-messenger perspective.

NGC 1068 is a very nearby spiral galaxy shown to have "bright emission and absorption lines" more than a century ago[7]. In 1943 Carl Seyfert noticed that "six extragalactic nebulae" had "high-excitation nuclear emission lines [...] broadened, presumably by Doppler motion"[8]. The list included NGC 1068 and NGC 4151. Seyfert galaxies, as they came to be known, are characterized by strong hydrogen, oxygen and neon emission lines (and other elements) and divided into two main classes: Seyfert Is and Seyfert IIs. The latter are sources with only narrow lines, while the former also have broad lines; the boundary is drawn at 1,000 km s^{-1} and is applied at the so-called full-width at half-maximum of the emission lines. This division is not simply semantic but, at the same time, turned out to be only apparent: in a seminal paper, Antonucci and Miller showed that the two classes represented the same types of source seen at different angles[9]. NGC 1068, the prototype Seyfert II, turned out in fact to have broad lines but only in polarized light (due to scattering, probably by free electrons). The picture that was put forwards was one of dust in a doughnut-like configuration, the so-called torus, surrounding the accretion disk on scales larger than those emitting the broad lines. In Seyfert IIs, which are observed edge-on with respect to the torus, only narrow emission lines (emitted farther away than the broad lines and therefore less Doppler-broadened) could be observed in the optical spectrum. The inner regions of Seyfert IIs are therefore much more obscured and absorbed than Seyfert Is. This also led to the birth of 'unified schemes', which unify apparently different, but intrinsically similar, classes of active galactic nucleus (AGN). With the discovery of quasars[10], Seyfert galaxies were shown to belong to the small fraction (~1%) of galaxies in which matter falling onto the central black hole converts its gravitational energy into radiation with the result that their nuclei become 'active' and can easily outshine their host galaxies[11]. Much less than 10% of all AGN become 'jetted'[12,13] and develop strong, long, relativistic jets—that is, structures in which matter is expelled at very high speeds, close to the speed of light, in relatively narrow beams.

Multi-messenger view

In this Review we assume a luminosity distance $D_L = 10.1$ Mpc (Supplementary Information). This means that 1″ corresponds to 48.9 pc and the black hole mass[14] (which scales like the linear size r given that in this case it is $\propto r v^2$, where v is the velocity) can be estimated to be $M_{\rm BH} = 6.7 \times 10^6$ solar masses ($M_\odot$) (see the discussion in ref. 15 of the robustness of this value), which implies an Eddington luminosity $L_{\rm Edd} \approx 8.4 \times 10^{44}$ erg s^{-1}.

As it is so close, NGC 1068 can be spatially resolved into a number of components, all of which maybe be relevant to neutrino production: (1) a starburst (SB) region in the spiral arms of its host galaxy; (2) an approximately kiloparsec long jet; (3) a sub-kiloparsec molecular outflow; and (4) the black hole vicinity (the accretion disk and perhaps the so-called corona). These can be studied by using observations in different electromagnetic bands, which provide complementary windows on the relevant physics.

Before discussing the multi-wavelength properties, we first show the integrated multi-messenger spectral energy distribution (SED) in Fig. 2. A number of features have been highlighted: (1) the $\nu^{-0.7}$ radio spectrum; (2) a template for the spiral host galaxy emission; (3) a template for the accretion disk plus X-ray corona emission; and (4) the γ-ray and neutrino bands. Given the vicinity of this source, its SED is largely due to the host galaxy, apart from the X-ray band.

Radio band and jet power

Figure 3 provides a beautiful overview of the inner few kiloparsecs of NGC 1068 at 1.7 GHz (18 cm; ref. 16). The radio continuum image shows an ~2-kpc-diameter SB disk (also detectable with molecular tracers[17]), and what looks like an ~500-pc-scale radio jet that terminates in lobes. The central 1″ further resolves into an approximately 50-pc-scale jet and compact radio knots (with the central engine believed to be close to component S). Note that the jet is almost two orders of magnitude shorter and much slower than the 'iconic' M87 jet (<0.05 c versus >0.99 c; refs. 18,19), for example, which implies that NGC 1068 is a 'non-jetted' AGN according to the classification proposed in ref. 13. We also point out that ref. 20 suggested that the velocities and trajectories of the radio flux peaks deviate from the expected behaviour of emission originating from a relativistic radio jet. Instead, they seem to be linked to larger structures associated with the host gas reservoir. In other words, the extended radio structures seen in this AGN could also easily be by-products of local shocks.

https://doi.org/10.1038/s41550-024-02339-z

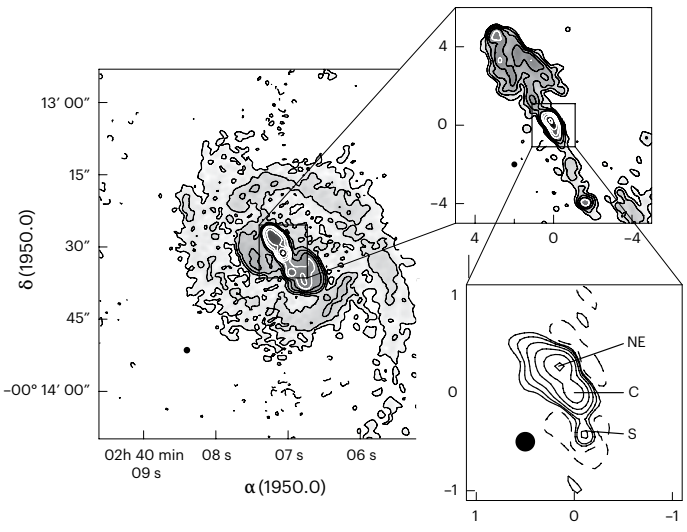

Fig. 3 | Aperture synthesis image of NGC 1068 at 1.7 GHz. Contours are overlaid on grayscale with a logarithmic stretch. The beam size (full-width at half-maximum) is indicated by a darkened ellipse located to the lower left of each panel. Right ascension (α) and declination (δ) coordinates are given at the 1950 epoch. Left: the SB disk. Top right: the radio jet. Bottom right: the central core, where NE, C, and S denote three radio components. In the two right panels the axes are offsets from component C in arcseconds. 1″ corresponds to 48.9 pc. Figure reproduced from ref. 16 under a Creative Commons license CC BY 4.0.

The total radio power at 1.4 GHz ($L_{\rm jet,1.4GHz}$) is 5.9×10^{22} W Hz^{-1} (using the NRAO VLA Sky Survey radio flux density[21]), which makes NGC 1068 a moderately luminous Seyfert galaxy. The power per unit frequency is commonly used in radio astronomy: it can be converted to ergs per second at 1.4 GHz by multiplying by 1.4×10^{16}. The shape of the radio continuum (Fig. 2) indicates synchrotron emission, which does not help in figuring out its origin, as both SB and jets can produce it. However, one can derive the relative contributions of the two components and then estimate the total jet power, $L_{\rm jet}$, from $L_{\rm jet,1.4GHz}$ to obtain $L_{\rm jet} = 10^{42.9\pm1.0}$ erg s^{-1} (Supplementary Information). For comparison, TXS 0506+056, the blazar that is the only other extragalactic source associated with IceCube neutrinos, has $L_{\rm jet} \approx 10^{45} - 4 \times 10^{46}$ erg s^{-1} based on SED modelling[22].

In principle both the jet and the SB region can be neutrino emitters through the interaction of high-energy protons with photons and/or protons, as discussed in detail in the 'Teraelectronvolt neutrino band' section.

Sub-millimetre band and molecular outflow power

AGN not only accrete matter to sustain their tremendous activity but many (possibly most) of them also show large-scale outflows/winds of matter driven by the central black hole (for example, refs. 23,24 and references therein), which are both less collimated and slower than relativistic jets. These play a major role in galaxy evolution through so-called AGN feedback (see ref. 25 for a review). Such large-scale outflows may in fact quench star formation and starve the AGN through a lack of fuel. AGN outflows come in various 'phases' that are characterized by different temperatures and compositions, such as ionized, atomic and molecular. These multiphase wide-angle winds have velocities ranging from ~10^2 km s^{-1}, typical of warm absorbers, up to semi-relativistic speeds of ~10^5 km s^{-1} for ultra-fast outflows (UFOs), and are observed at different spatial scales (sub-parsec to kiloparsec) and ionization states[24].

Most of the molecular gas in the interstellar medium (ISM) exists in the form of molecular hydrogen (H_2). H_2, however, is invisible in the cold ISM where the majority of the molecular gas is located and where sub-millimetre observations are sensitive to it (as its transitions can only be excited in warm regions probed by infrared (IR) or UV observations). The second most abundant molecule in the ISM, CO, is the best tracer of the global molecular reservoir at sub-millimetre wavelengths. At present, the Atacama Large Millimeter Array (ALMA), with its unprecedented sensitivity and spatial resolving power, is the most powerful tool for probing the molecular content in this band.

A massive molecular outflow in NGC 1068 has been revealed by ALMA observations[17,26] with tracers including CO and hydrogen cyanide (HCN), and has been associated with AGN feedback. This outflow also induces molecular shocks at the circumnuclear disk (CND, ~300-pc-scale; see (for example) refs. 27–29).

The kinetic power $L_{\rm kin}$ related to a multi-conical outflow can be estimated from the following expression (refs. 17,30):

$$L_{\rm kin} = \frac{3\,M_{\rm out}\,v^3}{2\,R_{\rm out}} \frac{\tan(\alpha)}{\cos(\alpha)^2}, \quad (1)$$

where $M_{\rm out}$ and $R_{\rm out}$ are the mass and radius of an outflow with velocity v and α is the angle between the outflow axis and the line of sight. Using updated values for the distance and $\alpha \approx 55°$ (as the inclination is $i \approx 35°$ from HyperLeda and i and α are complementary if the outflow is co-planar with the galaxy disk) and taking into account the uncertainties in the CO to H_2 conversion factor, α and $M_{\rm out}$, we derived what we consider to be a realistic estimate of $L_{\rm kin} = 10^{41.6\pm1.0}$ erg s^{-1}. The protons accelerated by the molecular outflow shocks can generate γ-rays and neutrinos through the same process mentioned in the 'Teraelectronvolt neutrino band' section (for example, ref. 31). However, such energetic processes could also dissociate some of the molecules in the medium, and this effect is not taken into account in existing modelling schemes.

Near-IR band and the torus

The Seyfert II nature of NGC 1068 implies the presence of a dusty torus, expected to be a few parsecs in size and thus surrounding the accretion disk but lying within the CND. The torus substantially obscures the inner region of NGC 1068 along our line of sight. With an accretion disk temperature of ~10^4–10^6 K, the bulk of its emission is in the optical and UV bands and is susceptible to absorption by dust. If the column density through the torus is high enough ($N_{\rm H} > 10^{24}$ cm^{-2}), even hard X-ray photons will get absorbed. All of this radiation is then reprocessed by nearby dust grains located close to the disk and re-emitted in the IR range with a similar power (see the 'X-ray band and AGN power' section). The exact geometry and structure of the torus are still topics of debate and early observational work and recent modelling suggest a more complicated structure compared with the original homogeneous doughnut shape (for example, refs. 32–34). Given its expected small size, the torus can only be observed by interferometers with ~100 m baselines, and NGC 1068 has been a prime target for the new IR interferometric instruments GRAVITY (K band, 2.2 μm) and Multi-AperTure mid-Infrared SpectroScopic Experiment (MATISSE) (L, M and N bands, 3–13 μm) at the European Southern Observatory/Very Large Telescope Interferometer in Cerro Paranal, Chile.

GRAVITY and MATISSE have now both confirmed the existence of, and resolved, the prominent dusty structure within the central few parsecs of NGC 1068. GRAVITY first resolved the K-band emission into a thin, ring-like structure with a radius of 0.17 pc, which has been interpreted as the inner, hot edge of the torus with a thin disk morphology[35]. In the nearby L, M, and N bands, MATISSE has imaged the larger-scale (up to 3 pc) colder dust into two distinct asymmetric structures with one extending in the polar directions[36]. Combining the two datasets, and fitting SEDs over multiple bands, suggests that the K-band emission may arise mostly from the far side of the structure. The conclusion is that the torus is composed of a parsec-scale inclined and optically thick inner disk and a prominent dusty outflow that connects to the outflow seen in molecular gas (see the 'Sub-millimetre band and molecular outflow power' section). This lends support to the current theoretical

picture of the torus as a disk plus wind complex, and confirms the need for strong corrections to derive the true power of the central AGN in NGC 1068 to take absorption into account.

X-ray band and AGN power

The X-ray band is key to studying AGN because X-ray emission seems to be (near) universal and X-rays are able to penetrate through high column densities of gas and dust, particularly at higher energies (≳10 keV: for example, ref. 37). Because of the rapid variability, X-rays can also temporally resolve the innermost parts of AGN that cannot be resolved spatially with current technology[38].

The general consensus is that very hot electrons (temperature $T \approx 10^9$ K) inverse Compton scatter the UV photons from the accretion disk, thereby producing X-ray photons. By analogy with stellar sources, the X-ray radiating zone is also called the corona[39]. While its location has to be close to the disk, its detailed structure, plasma composition and origin are not yet fully understood[40]. In fact, many possible corona structures have been proposed in the literature (see fig. 10 of ref. 41). Recent measurements obtained by the Imaging X-ray Polarization Explorer in Seyfert galaxies are challenging the commonly adopted lamp-post geometry (that is, a point-like corona illuminating a thin disk), favouring instead extended coronal geometries on/above the plane of the accretion disk[42–44].

The X-ray band is also important for estimating the bolometric luminosity, $L_{\rm bol}$, a key AGN parameter, whose determination requires a wealth of multi-wavelength data that are not always available. This is particularly true for Seyfert IIs, in which most of the AGN radiation is absorbed by dust and gas. While NGC 1068 is on average absorbed by column densities in excess of 10^{25} cm^{-2}, preventing a direct view of the intrinsic X-ray continuum, extensive monitoring campaigns with the Nuclear Spectroscopic Telescope Array (NuSTAR) detected an excess above 20 keV in some observations, suggesting unveiling events of the nucleus most probably due to a change in the absorption along the line of sight[34,45]. This enabled the only direct measurement of the coronal X-ray emission of NGC 1068: $L_{2-10\rm keV} = 3^{+3}_{-2} \times 10^{43}$ erg s^{-1}.

One can then use the so-called X-ray bolometric correction $K_{\rm x} = L_{\rm bol}/L_{\rm x}$. Using table 1 of ref. 46 and $L_{2-10\rm keV}$ from the paragraph above we derive $L_{\rm bol,x} = 10^{44.5\pm0.4\pm0.3}$ erg s^{-1} (where the first error term stems from the uncertainties on $L_{2-10\rm keV}$ and the second is the spread of the correlation). Using a calibration based on the [O IV] 25.89 μm line luminosity, ref. 47 estimated $L_{\rm bol,IR} = 10^{44.78}$ erg s^{-1}. This yields a logarithmic mean of $10^{44.7\pm0.5}$ erg s^{-1}, which is the value of $L_{\rm bol}$ we adopted here, ~400 times higher than the all-flavour isotropic neutrino luminosity (see the 'Teraelectronvolt neutrino band' section). (This is fully consistent with the logarithmic mean of the two extreme values given by ref. 35; that is, $L_{\rm bol} = 10^{44.8\pm0.5}$ erg s^{-1}). We then derived $L_{\rm bol}/L_{\rm Edd} \approx 0.6$, considering the black hole mass adopted in the 'Multi-messenger view' section, which is quite large for a local AGN.

Gamma-ray band and SB power

A γ-ray source at the position of NGC 1068 was initially reported in 2010 in the first Fermi Large Area Telescope (LAT) catalogue (1FGL)[48] and then associated with NGC 1068 (ref. 49). Since then, NGC 1068 has been included in every Fermi-LAT catalogue, up to 4FGL-DR4, at an increasing level of significance[50]. Its average power in the 0.1–100 GeV range over 12 years is $L_\gamma = 10^{40.92\pm0.03}$ erg s^{-1}, ~15 times smaller than the all-flavour isotropic neutrino luminosity (albeit in a different energy range; see the 'Teraelectronvolt neutrino band' section).

In the very-high-energy band, the source was observed by ground-based Cherenkov telescopes[51–53] resulting in no detection. The most stringent constraints on the very-high-energy flux were placed by a 125-h-long observation performed by the Major Atmospheric Gamma-ray Imaging Cherenkov (MAGIC) telescopes, which provided a 95% confidence level upper limit on the γ-ray flux above 200 GeV of 5.1×10^{-13} cm^{-2} s^{-1} (ref. 52).

The gigaelectronvolt γ-ray emission of NGC 1068 has been interpreted as being due to star-formation activity[54], which, through the creation of stellar remnants such as pulsars, pulsar-wind nebulae and supernova remnants, leads to the acceleration of cosmic rays. Their interaction produces γ-rays. In SB galaxies like NGC 1068 (Supplementary Informationx), most of this emission is of hadronic origin and produced via p–p interactions and the decay of neutral pions[55]. Star-forming galaxies are known to follow an L_γ–$L_{\rm IR}$ correlation where both luminosities are tracers of star-formation activity. The agreement of NGC 1068 with this correlation and the lack of variability of γ-rays (for example, refs. 54,56) support the interpretation that the majority of the emission is related to star-formation activity.

A contribution to the γ-ray emission could, in principle, come from a UFO in NGC 1068. Indeed, ref. 57 reported the detection of γ-rays from a sample of nearby AGN with a UFO. Adopting the scaling relations in ref. 57 and estimating $L_{\rm kin} \lesssim 10^{43}$ erg s^{-1} from the $L_{\rm kin}$–$L_{\rm bol}$ relationship of ref. 58, one can derive a range for the UFO γ-ray luminosity of between $10^{39.6\pm1.0}$ erg s^{-1} and $10^{41.2\pm1.0}$ erg s^{-1}, where the uncertainties take into account the errors in the scaling relations of ref. 57. Note that, while the UFO may explain (and actually overshoot) the γ-ray luminosity of the source, there is no robust evidence that such a UFO exists in NGC 1068, as UFOs are nearly impossible to detect in X-rays in heavily obscured AGN, where direct observation of the intrinsic nuclear continuum in the Fe K band is hindered[59].

On the other hand, as shown in the 'Sub-millimetre band and molecular outflow power' section, NGC 1068 exhibits a massive molecular outflow with an outflow rate of ~38 $M_\odot$ yr^{-1}. Gamma-ray emission has been observed from a sample of nearby galaxies (including NGC 1068) with a molecular outflow[60]. Contrary to the UFO case, however, no correlation was found between $L_{\rm kin}$ and L_γ, which makes it impossible to estimate any contribution from the molecular outflow to the γ-ray emission.

The γ-ray emission from the jet is very probably negligible as NGC 1068's jet is not as strong and fast (see the 'Radio band and jet power' section) as the relativistic jets in the sources typically detected by Fermi-LAT—that is, blazars, which are also very variable. In fact, if we assume the same $L_\gamma/L_{\rm 1.4GHz}$ ratio as the blazar TXS 0506+056 (ref. 61), where both powers are jet-related, $L_{\gamma,\rm jet}$ in NGC 1068 should be ~70 times higher than observed (or ~7 times in the less extreme case of an M87-like jet).

Teraelectronvolt neutrino band

The IceCube result was the outcome of a new and improved analysis of 9 years (2011–2020) of neutrino event candidates that were updated with newer processing and detector calibrations[62]. The search that led to the detection of significant neutrino emission from NGC 1068 tested 110 γ-ray emitters[63] defined a priori and located in a declination range covering the northern sky, $-3° < \delta < 81°$. The selected objects included 95 blazars, 5 AGNs, 9 other types of galaxies and 1 Galactic source[6]. Dedicated searches in the direction of pre-defined source candidates are not new to the IceCube analyses (see, for example, ref. 64). The selection method used to identify the 110 interesting candidates selected in ref. 6 was the same as that used in a previous IceCube analysis[65] that reported a 2.9σ excess from the direction of NGC 1068. The most significant object in the list was again NGC 1068, and indeed the most significant location identified by the scan of the Northern Hemisphere was found only 0.11° away from this source (Fig. 1). The muon–neutrino energy flux from NGC 1068 at 1 TeV under the assumption of a single power law had a best-fit normalization $\Phi^{1\,\rm TeV}_{\nu_\mu+\bar\nu_\mu} = (5.0 \pm 2.1_{\rm stat+sys}) \times 10^{-11}$ TeV^{-1} cm^{-2} s^{-1} and a best-fit spectral index $\Gamma = 3.2 \pm 0.3_{\rm stat+sys}$, valid in the energy range between 1.5 and 15 TeV, where we have included the statistical and systematic uncertainties. This flux corresponds to an equivalent all-flavour isotropic neutrino luminosity $L_\nu = 10^{42.1\pm0.2}$ erg s^{-1} in the same energy range.

https://doi.org/10.1038/s41550-024-02339-z

Table 1 | Measured powers

L_{radio} (1.4 GHz) (erg s^{-1})	L_{FIR} (8–100 μm) (erg s^{-1})	L_x (2–10 keV) (erg s^{-1})	L_γ (0.1–100 GeV) (erg s^{-1})	L_ν (1.5–15 TeV) (erg s^{-1})	L_{Edd} (erg s^{-1})
$10^{38.9}$	$10^{44.6\pm0.1}$	$10^{43.4\pm0.3}$	$10^{40.92\pm0.03}$	$10^{42.1\pm0.2}$	$10^{44.9\pm0.3a}$

[a]A factor of 2 uncertainty was assumed on M_{BH}.

Table 2 | Derived powers

L_{kin} (erg s^{-1})	L_{jet} (erg s^{-1})	L_{bol} (erg s^{-1})	L_{bol}/L_{Edd}
$10^{41.6\pm1.0}$	$10^{42.9\pm1.0}$	$10^{44.7\pm0.5}$	$10^{-0.3\pm0.6}$

Note that the Eddington ratio is unitless.

Table 3 | Estimated γ-ray and neutrino powers

Component	Scale	L_γ(0.1–100 GeV) (erg s^{-1})	L_ν(1.5–15 TeV) (erg s^{-1})
Star formation	>kiloparsec	~$10^{40.9}$	$\lesssim 10^{40.1}$
Jet	~kiloparsec	<$10^{41.7}$ (M87-like)	<$10^{40.9}$
Outflow (UFO)	~parsec	<$10^{41.2}$	<$10^{40.4}$
Black hole vicinity	~0.03 mpc (~50 R_s)	?	?
Total		$\lesssim 10^{41.9}$	$\ll 10^{41.1}$
Observed		$10^{40.92\pm0.03}$	$10^{42.1\pm0.2}$

R_s is the Schwarzschild radius. '?' denote unknown values.

High-energy neutrinos are generated in the decay of charged pions, which are in turn produced when cosmic rays interact with ambient matter (p–p) or low-energy radiation (photohadronic (p–γ) interactions). The final products of the decay chain of a charged pion:

$$\pi^{\pm} \rightarrow \mu^{\pm} + \nu_{\mu}(\bar{\nu}_{\mu}) \tag{2}$$

$$\mu^{\pm} \rightarrow e^{\pm} + \bar{\nu}_{\mu}(\nu_{\mu}) + \nu_e(\bar{\nu}_e) \tag{3}$$

are four stable particles: one electron (or positron) and three neutrinos and antineutrinos[66,67].

Neutral pions are also produced in p–p and p–γ interactions, in approximately the same amounts as charged ones, decaying into two γ-rays, $\pi^0 \rightarrow \gamma + \gamma$. The energy of the pions (both charged and neutral) is shared roughly equally among the final products of the decay, and this has two important consequences: (1) a flux of neutrinos from astrophysical sources is unavoidably accompanied by a γ-ray flux $F_\gamma \approx 2 \times F_\nu$; (2) the energies of a neutrino (E_ν) and of a photon (E_γ) generated in cosmic ray interactions are proportional to the cosmic ray proton energy E_p and related by $E_\gamma \approx 2 \times E_\nu$ (refs. 66,67).

Relevant powers and the case for a 'hidden' source scenario

Tables 1 and 2 summarize the relevant powers discussed in this Review; we distinguish between 'measured' (radio, far-infrared (FIR), X-ray, γ-ray, neutrino and Eddington) and 'derived' (outflow, jet, bolometric and Eddington ratio) values respectively.

Having examined all available data, both in the electromagnetic and neutrino bands, we next address the question of the origin of the neutrino emission. Our starting point is the fact that NGC 1068 is much weaker in teraelectronvolt photons than in neutrinos (see the upper limits in Fig. 2 and the 'Gamma-ray band and SB power' and 'Teraelectronvolt neutrino band' sections).

Table 3 puts this statement into perspective by estimating the maximum neutrino power that can be associated to the various components. This was done by making three extreme assumptions: (1) γ-ray photons are fully hadronic (hence $L_\nu \approx L_\gamma/2$); (2) L_γ is as large as possible; (3) the conversion between the Fermi and IceCube bands is done assuming $\Gamma_\nu = 2$ (while the observed one is $\Gamma_\nu = 3.2$), which implies, together with assumption number (1), that L_ν(1.5–15 TeV) ≈ L_γ(0.1–100 GeV)/6. Any deviation from these premises will result in lower neutrino powers. While the star-formation-related L_γ is the observed one, we have maximized the γ-ray emission associated with the two other components by assuming an absorbed M87-like jet power, which is completely unphysical, and the maximum possible value for a UFO for the outflow (see the 'Gamma-ray band and SB power' section). The resulting neutrino power must then be $\ll 10^{41.1}$ erg s^{-1} – that is, more than a factor of ten less (realistically at least two orders of magnitude using only the star-formation component) than the IceCube value. As in a photohadronic scenario neutrinos are associated with a γ-ray flux that is twice as high and twice as energetic, Fig. 2 implies that the photons related to neutrino production have an intrinsic flux ~40 times higher than the MAGIC upper limits (see the 'Gamma-ray band' section) and therefore need to be totally absorbed.

We next evaluate the characteristics that the emission region must possess to meet the criteria derived above. We focus here on the p–γ scenario as it provides a very natural explanation for both the neutrino flux and the low level of γ-ray emission. We remind the reader, however, that if the gas density is large enough, a p–p origin of high-energy neutrinos cannot be ruled out.

The p–γ cross-section is characterized by a pronounced peak just above the threshold for pion production[68]. For well-behaved photon spectra, most p–γ interactions occur near the threshold and result in the production of a single pion, either charged or neutral (multiple-pion production takes over at larger energies). Moreover, the incident proton loses a fraction m_π/m_p (the ratio of the pion to proton mass) of its energy in each interaction and the characteristic energy of each neutrino is $E_\nu \approx (m_\pi/4m_p)E_p \approx 0.04 \times E_p$, where the factor of four represents the number of stable particles resulting from the interaction[66].

The neutrinos observed by IceCube are therefore generated by cosmic ray protons of energy ~40–400 TeV. Owing to the threshold condition, to actually produce neutrinos protons must interact with photons of energy:

$$\epsilon_\gamma^{th} \gtrsim 2\,(E_p/40\ \mathrm{TeV})^{-1}\ \mathrm{keV}, \tag{4}$$

that is, in the X-ray domain.

Neutrino production in a photon-rich environment would also remarkably explain the flux suppression in γ-rays due to the onset of pair production in the ambient radiation field, provided that the threshold condition $E_\gamma \epsilon_\gamma > (m_e c^2)^2$ is satisfied[69,70]. This translates into a minimum energy:

$$\epsilon_\gamma > 0.26\,(E_\gamma/\mathrm{TeV})^{-1}\ \mathrm{eV}, \tag{5}$$

that is, in the IR domain (wavelength $\lambda < 4.8$ μm) and above (energy wise).

The conditions required by equations (4) and (5) are easily satisfied very close to the supermassive black hole at the centre of the AGN, a region that provides X-ray and optical/IR photons in abundance[71]. The X-ray corona (see the 'X-ray band and AGN power' section) in particular has been singled out as the region responsible for neutrino emission (see the 'Nailing down the hidden source case' section).

Electron–positron pairs generated this way will inverse Compton scatter ambient photons up to the γ-ray domain, thereby initiating an electromagnetic cascade that is sustained by alternate inverse Compton and pair-production processes. The cascade reaches its natural end when the typical energy of photons equals the threshold for pair production: $E_\gamma^{th} = (m_e c^2)^2/\epsilon_\gamma$. The electron/positron generated in the last pair-production event will have an energy $E_e^{min} \approx E_\gamma^{th}/2$, and will inverse Compton upscatter ambient photons to an energy

$E_\gamma^{esc} = (4/3)(E_e^{min}/m_e c^2)^2 \epsilon_\gamma = E_\gamma^{th}/3$. Photons of such energy are unable to pair-produce in the ambient photon gas, and will freely escape the region[66].

The spectrum of ambient photons in the AGN corona extends well into the kiloelectronvolt range. These X-rays, which are the targets for neutrino production, are also the reason why the AGN corona remains opaque for gigaelectronvolt γ-rays, given that the pair-production cross-section is much larger than that of pion production. Runaway photons escaping from this environment need to have at most megaelectronvolt energies, $E_\gamma^{esc} \approx 45\,(\epsilon_\gamma/2\,\mathrm{keV})^{-1}$ MeV, which are in an energy range that has so far been very poorly explored. Future megaelectronvolt missions, such as the All-sky Medium-Energy Gamma-ray Observatory eXplorer (AMEGO)-X[72] and the enhanced ASTROGAM (e-ASTROGAM)[73], are therefore of paramount importance, as they may be the only instruments capable of revealing the electromagnetic counterpart of neutrino sources similar to NGC 1068.

The same conclusion would be reached in a scenario where the electromagnetic cascade is completely suppressed due to the presence of a magnetic field[74]. If the ambient magnetic field is strong enough, multi-teraelectronvolt cosmic rays would produce teraelectronvolt electrons and such electrons would cool through synchrotron emission, rather than inverse Compton/pair-production processes. For a kilogauss field, as might be found in AGN coronae (see the 'AGN corona' section), the energy of the synchrotron photons falls in the megaelectronvolt domain, $\epsilon_{syn} \approx 20(B/\mathrm{kG})(E_e/\mathrm{TeV})^2$ MeV (see, for example, ref. 75).

Nailing down the hidden source case

The existence of neutrino sources not associated with any (except for megaelectronvolt) photon counterpart (and therefore named hidden sources) was first predicted in the 1970s in a number of pioneering papers[76–78]. NGC 1068 is the first such source to be detected, and this revived interest in modelling neutrino production in environments opaque to high-energy radiation[79,80].

We now expand on the previous section and establish theoretical connections between the primary candidate astrophysical sites, particle acceleration and interactions, summarizing the multi-messenger implications for NGC 1068.

Star-forming region

Star-forming regions and SBs are powerful cosmic ray factories due to high supernova rates, which in turn is a result of enhanced star-formation rates. Given that it is the seed of star formation, a high gas density ($n \gtrsim 10^2\,\mathrm{cm}^{-3}$) is typically found in star-forming environments. Such a density is high enough to make the inelastic p–p interaction rate comparable to, or more efficient than, the escape rate. Therefore, copious production of γ-rays and high-energy neutrinos is expected (see the 'Teraelectronvolt neutrino band' section). The star-formation environment possesses also a strong FIR dust emission (with a radiation energy density $U_{RAD} \gtrsim 10^3\,\mathrm{eV\,cm}^{-3}$) resulting from the efficient absorption of starlight, which is reprocessed at lower frequencies. This photon background is responsible for efficient $\gamma\gamma$ absorption of ≳10 TeV photons, while those at lower energies are unabsorbed (equation (5)).

The gigaelectronvolt γ-ray luminosity of NGC 1068 is roughly compatible with what can be expected from the FIR–γ-ray correlation (see the 'Gamma-ray band and SB power' section). Therefore, the SB is an interesting candidate for explaining the bulk of the observed gigaelectronvolt γ-rays. NGC 1068 is characterized by a SB ring of radius ≈ 1 kpc and a CND. Reference 81 found that the inner CND cannot explain the γ-ray data without overproducing the radio constraints. However, ref. 82 pointed out that the SB ring features the right conditions to be consistent with the multi-wavelength observations, but cannot be the main source of the IceCube neutrino flux. Finally, ref. 82 and ref. 56 reported that NGC 1068's 20 MeV–1 TeV spectrum can be interpreted as the sum of two hadronic components: a highly obscured one related to the AGN and responsible for the ≲500 MeV emission and another produced in the SB ring by star-formation activity.

AGN outflow

AGN outflows/winds (see the 'Sub-millimetre band and molecular outflow power' and 'Gamma-ray band and SB power' sections) may be launched from the accretion disk by several mechanisms involving thermal, radiative and magnetic processes. During propagation, AGN-driven winds, similarly to other diverging flows, are expected to develop a structure that is characterized by an inner wind termination shock and an outer forward shock. As discussed in the following paragraphs, both have been proposed as possible sites for particle acceleration through diffusive shock acceleration.

Particle acceleration at the forward shock of the AGN-driven molecular wind observed in NGC 1068 is strongly constrained by the upper limits on the γ-ray flux in the very-high-energy band obtained by the MAGIC telescopes (see the 'Gamma-ray band and SB power' section). This outflow expands at a large distance in the host galaxy and p–p inelastic collisions are the main production mechanism for γ-rays and neutrinos. This model predicts a maximum neutrino event rate of ~0.07 yr^{-1}, which is much lower than that observed by IceCube[31].

Parsec- and sub-parsec-scale fast winds, such as UFOs, could also be present in the nuclear region of NGC 1068. However, the Compton-thick nature of such a nuclear region makes the detection of such winds extremely challenging (see the 'X-ray band and AGN power' and 'Gamma-ray band and SB power' sections). In a small-scale wind such as a UFO p–p and p–γ interactions could account for the γ-ray emission observed in the Fermi-LAT band, while their contribution to the IceCube neutrino flux would be limited to <10% (ref. 83).

Finally, a scenario in which neutrinos are produced in the inner regions of a failed wind (that is, a wind that never reaches the local escape velocity) was also investigated[84]. In this context neutrinos are mainly generated via p–γ interactions with the AGN radiation field, and the predicted neutrino flux is as high as that observed by IceCube above 1 TeV. This scenario shares some similarities with the AGN corona models (see the 'AGN corona' section), such as the spatial scale of the neutrino production site and the vicinity to the emission region of the target X-ray AGN photon field. This system is optically thick for gigaelectronvolt–teraelectronvolt γ-rays. As for the corona case, to reproduce the observed γ-ray spectrum in the Fermi-LAT band, a separate external emission region must be postulated—that is, a larger-scale wind or the SB ring.

Jet

NGC 1068 has a weak and slow jet with a kinetic luminosity $L_{jet} \approx 10^{43}\,\mathrm{erg\,s}^{-1}$ (see the 'Radio band and jet power' section). Reference 49 proposed a leptonic scenario for the observed gigaelectronvolt flux with an artificial broken power-law spectrum of relativistic electrons that extends up to 0.5 TeV and inverse Compton scatters IR photons from the torus within parsec-scale blob structures. However, the lack of time variability of the γ-ray flux (see the 'Gamma-ray band and SB power' section) and the need for a distinct acceleration-cooling scenario, as pointed out by ref. 85, make a leptonic jet interpretation unlikely. In this context, a hadronic counterpart is disfavoured to explain a sizable fraction of the IceCube neutrino flux unless the proton-dominated emission is spatially and energetically decoupled from the associated leptonic component and localized in an optically thick region. Such a scenario is discussed by ref. 86 for certain knot structures within the jet, where a peak in the γ-ray energy spectrum between 100 GeV and 1 TeV, as well as a dominant neutrino flux contribution above ~10 TeV, is predicted if the proton energy spectrum is sufficiently hard. The possible cosmic ray production site in the head of the jet[87] yields another potential hadronic contribution to the γ-ray energy spectrum that could become dominant above a few

https://doi.org/10.1038/s41550-024-02339-z

gigaelectronvolts[85]. The entire spectrum of the observed γ-rays, however, cannot be explained by any of these structures within the jet.

AGN corona

As discussed in the 'Relevant powers and the case for a 'hidden' source scenario' section, the large discrepancy between neutrino and γ-ray powers (see also Fig. 2 and Tables 1 and 3) requires a high γ-ray opacity. This is accommodated relatively naturally if the acceleration/interaction region is identified as the corona of the supermassive black hole (see the 'X-ray band and AGN power' and 'Relevant powers and the case for a 'hidden' source scenario' sections and ref. 80). The high temperature of the gas expected in the corona leads us to think that shock waves in this region should be relatively weak, thereby leading to steep spectra of the accelerated particles.

In this context, ref. 80 and ref. 79 respectively proposed stochastic acceleration in turbulence (a second-order Fermi process) and diffusive shock acceleration (a first-order Fermi process) as the main acceleration mechanisms. Both scenarios are able to produce a strong neutrino signal while the γ-ray counterpart is efficiently absorbed and reprocessed in the megaelectronvolt band (see also refs. 75,82,84).

AGN coronae are believed to extend for less than ~$10^2\,R_s$ and are characterized by an intense X-ray radiation field associated with the accretion activity. Some simple estimates can illustrate the rough properties of the corona: its radius can be parameterized as $R_c = \eta R_s$ (where $\eta \approx 10$–100), so that, assuming approximate virial balance between gravitational, thermal and magnetic energies, the proton temperature of the corona becomes $k_B T_p = m_p c^2/6\eta$ (where k_B is the Boltzmann constant)—that is, $T_p \approx 6.1\times10^{10}(\eta/30)^{-1}$ K. Note that this is about an order of magnitude larger than that of thermal electrons estimated from the cutoff in the observed X-ray spectra. Although some level of thermalization between protons and electrons is expected, the timescale for full equilibration between the two species is exceedingly long[88–90], and it is reasonable to expect that protons in the corona are much hotter than electrons.

The magnetic field in the corona can also be estimated as:

$$B = \sqrt{\frac{4\pi\rho_p}{3\eta\beta_P}}\,c = 2.2\times10^3\,\mathrm{G}\,(\eta/30)^{-1}M_7^{-1/2}\tau_T^{1/2}\beta_P^{-1/2}, \qquad (6)$$

where $\rho_p = n_p m_p$ is the proton mass density and $\beta_P = 8\pi n_p k_B T_p/B^2$ is the ratio between the magnetic and thermal energy densities (where the subscript P refers to the plasma). Here we introduced the Thomson opacity of the corona $\tau_T = n_p\sigma_T R_c$, M_7 as the black hole mass in units of $10^7\,M_\odot$, and we have used the results previously obtained for the gas temperature. From the definition of the Alfvén speed (v_A) one can see that in the corona $v_A/c_s \approx \beta_P^{-1/2}$ and $v_A = c/\sqrt{3\eta\beta_P}$, where c_s is the sound speed. The fact that v_A is close to the speed of light is an important ingredient to make turbulent particle acceleration efficient.

Interestingly, the spectrum of high-energy neutrinos measured from the direction of NGC 1068 is very steep, $\propto E_\nu^{-3.2}$. This piece of information is crucial to estimate the total luminosity in the form of accelerated particles necessary to power the neutrino signal. As discussed above, neutrino production at $E_\nu \approx 1$ TeV in p–p and p–γ reactions requires a proton with $E \approx 25$ TeV. Assuming that protons dump all their energy near the black hole, the observed neutrino luminosity requires a proton luminosity at energies >25 TeV of ~10^{42} erg s^{-1}. Extrapolating this down to 1 GeV, assuming the spectrum of the IceCube neutrinos, results in ~5×10^{46} erg s^{-1}. This number underestimates the real luminosity by a factor of at least around 2 (because of particles with $E < 1$ GeV). It is clear that if the steep spectrum of parent protons were to extend to low energies, then both L_{Edd} (Table 1) and L_{bol} (Table 2) would be exceeded (note also that in these estimates we neglected the energy required to feed the thermal and magnetic energy of the corona).

The most natural explanation for the steep neutrino spectrum is that it reflects the cutoff region of the parent protons, while the lower energy spectrum should be hard enough to avoid or alleviate problems with energetics.

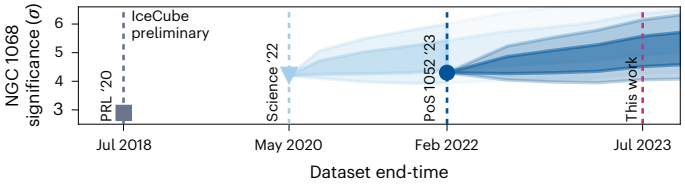

Fig. 4 | Expected increase in significance of neutrino emission from NGC1068 over time. The significance of IceCube detections is shown at various epochs, indicated by the vertical dashed lines. The result from ref. 65 (grey square) used different data processing and analysis methods. Starting from ref. 6 (light blue triangle), the projected significance is shown as light blue bands, with darker and lighter bands representing 68% and 95% containments respectively, assuming a steady neutrino flux as measured by IceCube and with an evolution based on the increased statistics only. The significance from ref. 98 (dark blue dot) is compatible with previous measurements within 1 σ. The dark shaded bands emanating from the blue dot illustrate the expected significance of future measurements assuming a steady flux as measured in ref. 98. Figure adapted from ref. 95 under a Creative Commons license CC BY-NC-ND 4.0.

These conclusions reflect on considerations regarding the specific acceleration process that is responsible for particle energization. Shocks in the environment associated with the corona are likely to have low Mach number, given the fact that the free fall velocity and the sound speed are very close to each other and the spectrum of accelerated particles is therefore expected to be much steeper than E^{-2} (alternatively, the entire corona could be the downstream region of a strong shock, so that particles could be accelerated elsewhere and eventually advected into the corona). As discussed above, while this result can be in line with the observed steep neutrino spectrum, it creates severe problems with global energetics. On the other hand, the high Alfvén speed in the corona suggests that stochastic acceleration may be at work. Such a process may naturally produce hard spectra with a cutoff energy consistent with the observed neutrino spectrum. This possibility is discussed in more detail in the Supplementary Information.

It is useful to point out that while magnetohydrodynamic simulations of the region near the black hole do not show evidence of shocks[91], they do suggest that a hot corona is formed above the accretion disk[92], lending support to the picture outlined above.

Recently, ref. 93 (see also ref. 94) explored relativistic magnetic reconnection as an alternative acceleration mechanism responsible for the injection in the corona of a hard proton spectrum ($\propto E^{-1}$) featuring a break at about 25 TeV. Such a scenario could offer a viable alternative and/or a complement to stochastic acceleration in providing the non-thermal proton population with the necessary energy to power the observed neutrino flux.

Outlook

The 4.2 σ evidence of teraelectronvolt neutrino emission from NGC 1068 (see the 'Teraelectronvolt neutrino band' section) combined with multi-wavelength observations (see the 'Radio band and jet power' to 'Gamma-ray band and SB power' sections), especially in the X-ray and γ-ray bands, could provide a new window on the high-energy and hadronic processes taking place in the innermost region(s) of AGN. Owing to the limited angular resolution of IceCube, this would not be possible with neutrinos alone. Several avenues complement each other in realizing this opportunity, some of which are already being pursued. As shown in Fig. 4, the significance of the neutrino observations from NGC 1068 could reach the discovery threshold of 5 σ, which is commonly used in particle physics, in upcoming work[95] that aims to extend the analysis from 9 to 13 years. According to preliminary projections, including refinements to the analysis

methods, the significance is expected to fall within 4.5 σ to 5.5 σ (68% confidence limit).

The extent to which the processes that produce neutrinos in NGC 1068 generalize to the wider AGN population is not yet known. It is therefore of the utmost importance to identify and study other neutrino-producing AGN. Assuming a connection with the plasma in AGN coronae, studies of Seyfert galaxies that host X-ray-bright AGN (after accounting for X-ray absorption) have been encouraged[96]. Owing to IceCube's markedly higher sensitivity to neutrino sources situated in the northern sky as opposed to those in the southern sky, the two regions are usually studied separately. Combining the model of refs. 80,96 with X-ray measurements reported by the BAT AGN Spectroscopic Survey[97], two corresponding IceCube searches are underway[98,99]. Promising targets have been identified, and include NGC 4151 and NGC 4388 in the north, as well as the Circinus Galaxy in the south. Preliminary results indicate that the data associated with the selection of Seyfert galaxies in the northern sky, particularly NGC 4151 and CGCG 420-015, are inconsistent with the neutrino background at the 2.7 σ level of significance, but not exactly as predicted by the combination of the chosen corona model[96] and the underlying X-ray measurements. For example, no potential signal was found for NGC 4388, thereby excluding the most optimistic model prediction of ~20 neutrinos at more than 90% confidence level[98]. These results motivate further studies with ample opportunities for exciting discoveries, but are insufficient to claim as evidence for the tested scenario. A third IceCube analysis, looking for a correlation between IceCube neutrinos and hard X-ray AGN in general, reported that NGC 4151 represents the most interesting candidate source with a preliminary significance of 2.9 σ (ref. 100). For Compton-thick AGN, the estimated intrinsic X-ray luminosities come with large systematic uncertainties that directly influence the predicted neutrino fluxes. The estimation can be improved by including NuSTAR data for such objects[101], although in most cases it would still be relatively model-dependent, as a direct view of the intrinsic luminosity is hampered even at very high energies. One example is NGC 3079, which may be brighter in neutrinos than estimated originally[102], adding to the growing indications of neutrino emission from AGN.

These ongoing efforts would benefit from observations of these candidate sources in the megaelectronvolt band by future facilities[72,73], as discussed in the 'Relevant powers and the case for a 'hidden' source scenario' section, and reduced uncertainties in the distance estimates of nearby AGN. Moreover, future neutrino detectors in the Northern Hemisphere, such as GVD (https://baikalgvd.jinr.ru/), KM3NeT (https://www.km3net.org/), P-ONE (https://www.pacific-neutrino.org/) and TRIDENT (https://trident.sjtu.edu.cn/en), will be vital to provide stronger constraints on interesting targets in the southern sky.

Conclusions

The detection of IceCube neutrinos from NGC 1068 was surprising because non-jetted AGN are typically dominated by thermal emission[11]. Contrary to early ideas[76–78], recent work has primarily focused on jetted AGN, known for their predominantly non-thermal emission, as potential sources capable of accelerating protons to the energies required for neutrino production.

NGC 1068 is a complex source with four distinct components: a SB, a jet, a molecular outflow and an active black hole. While each of these components could potentially be a source of neutrinos, a comprehensive analysis of the multi-messenger characteristics of this object led us to rule out the first three as possible neutrino emitters. This exclusion process ultimately points to the region near the black hole as the sole environment where both proton acceleration and photon interactions can occur at the required intensity.

It is worth noting that the cosmic rays that may be associated with NGC 1068 are of relatively mid-range energy (~40–400 TeV) compared with the much higher energies required for TXS 0506+056 (~800 TeV–90 PeV)[103]. This implies that non-jetted and jetted AGN might be complementary neutrino emitters, explaining at least part of the IceCube astrophysical background emission at the low- and high-energy ends, respectively.

The general scenario emerging from the multi-messenger study reported here can be then summarized as follows: (1) the powerful inner region, possibly the AGN corona, is required to explain neutrino emission through photohadronic interactions; (2) this same region can also provide the photon-rich environment needed to absorb the neutrino-associated γ-rays, as these have not been detected; (3) the outer region (SB, AGN wind) dominates the gigaelectronvolt γ-ray flux. It is important to keep in mind, however, that our knowledge of the X-ray corona is still limited, and this issue may not be entirely resolved.

We stress that the main conclusion we reach for NGC 1068, namely that the neutrino emitter must be hidden in a γ-ray-opaque environment, also applies to at least some of the sources responsible for the diffuse background emission observed by IceCube, as otherwise their γ-ray emission would violate the Fermi-LAT constraints on the isotropic γ-ray background[104].

Future observations in the megaelectronvolt energy band could probe the coronal activity, where the absorbed gigaelectronvolt–teraelectronvolt γ-rays are expected to be reprocessed. Further studies with IceCube and other neutrino observatories will help to constrain the connection between neutrinos and AGN, and reveal the nature of the central engine powering the region surrounding the supermassive black hole. In particular, the quest for the origin of the particles responsible for neutrino production, and more specifically their spectrum—a crucial parameter for assessing the energetics of the phenomena involved—would benefit from measurements of the neutrino flux down to energies <1 TeV, but this is very challenging from an observational point of view. Such a measurement would provide a direct test of the acceleration mechanisms discussed above.

References

1. Aartsen, M. G. et al. First observation of PeV-energy neutrinos with IceCube. *Phys. Rev. Lett.* **111**, 021103 (2013).
2. IceCube Collaboration. Evidence for high-energy extraterrestrial neutrinos at the IceCube Detector. *Science* **342**, 1242856 (2013).
3. Icecube Collaboration. Observation of high-energy neutrinos from the Galactic plane. *Science* **380**, 1338–1343 (2023).
4. IceCube Collaboration. Multimessenger observations of a flaring blazar coincident with high-energy neutrino IceCube-170922A. *Science* **361**, eaat1378 (2018).
5. IceCube Collaboration. Neutrino emission from the direction of the blazar TXS 0506+056 prior to the IceCube-170922A alert. *Science* **361**, 147–151 (2018).
6. IceCube Collaboration. Evidence for neutrino emission from the nearby active galaxy NGC 1068. *Science* **378**, 538–543 (2022).
7. Fath, E. A. The spectra of some spiral nebulae and globular star clusters. *Lick Obs. Bull.* **149**, 71–77 (1909).
8. Seyfert, C. K. Nuclear emission in spiral nebulae. *Astrophys. J.* **97**, 28 (1943).
9. Antonucci, R. R. J. & Miller, J. S. Spectropolarimetry and the nature of NGC 1068. *Astrophys. J.* **297**, 621–632 (1985).
10. Schmidt, M. 3C 273 : a star-like object with large red-shift. *Nature* **197**, 1040 (1963).
11. Padovani, P. et al. Active galactic nuclei: what's in a name? *Astron. Astrophys. Rev.* **25**, 2 (2017).
12. Padovani, P. The microjansky and nanojansky radio sky: source population and multiwavelength properties. *Mon. Not. R. Astron. Soc.* **411**, 1547–1561 (2011).
13. Padovani, P. On the two main classes of active galactic nuclei. *Nat. Astron.* **1**, 0194 (2017).
14. Greenhill, L. J., Gwinn, C. R., Antonucci, R. & Barvainis, R. VLBI imaging of water maser emission from the nuclear torus of NGC 1068. *Astrophys. J. Lett.* **472**, L21 (1996).

15. Wang, J.-M., Songsheng, Y.-Y., Li, Y.-R., Du, P. & Yu, Z. Dynamical evidence from the sub-parsec counter-rotating disc for a close binary of supermassive black holes in NGC 1068. *Mon. Not. R. Astron. Soc.* **497**, 1020–1028 (2020).
16. Gallimore, J. F., Baum, S. A., O'Dea, C. P. & Pedlar, A. The subarcsecond radio structure in NGC 1068. I. Observations and results. *Astrophys. J.* **458**, 136 (1996).
17. García-Burillo, S. et al. Molecular line emission in NGC 1068 imaged with ALMA. I. An AGN-driven outflow in the dense molecular gas. *Astron. Astrophys.* **567**, A125 (2014).
18. Roy, A. L., Wilson, A. S., Ulvestad, J. S. & Colbert, J. M. Slow jets in Seyfert Galaxies: NGC1068. In *Proc. 5th European VLBI Network Symposium* (eds Conway, J. E. et al.) 7 (Onsala Space Observatory, 2000).
19. Park, J. et al. Kinematics of the M87 jet in the collimation zone: gradual acceleration and velocity stratification. *Astrophys. J.* **887**, 147 (2019).
20. Fischer, T. C., Johnson, M. C., Secrest, N. J., Crenshaw, D. M. & Kraemer, S. B. No small-scale radio jets here: multiepoch observations of radio continuum structures in NGC 1068 with the VLBA. *Astrophys. J.* **953**, 87 (2023).
21. Condon, J. J. et al. The NRAO VLA Sky Survey. *Astron. J.* **115**, 1693–1716 (1998).
22. Ansoldi, S. et al. The blazar TXS 0506+056 associated with a high-energy neutrino: insights into extragalactic jets and cosmic-ray acceleration. *Astrophys. J. Lett.* **863**, L10 (2018).
23. Harrison, C. M. Impact of supermassive black hole growth on star formation. *Nat. Astron.* **1**, 0165 (2017).
24. Cicone, C. et al. The largely unconstrained multiphase nature of outflows in AGN host galaxies. *Nat. Astron.* **2**, 176–178 (2018).
25. Fabian, A. C. Observational evidence of active galactic nuclei feedback. *Annu. Rev. Astron. Astrophys.* **50**, 455–489 (2012).
26. Impellizzeri, C. M. V. et al. Counter-rotation and high-velocity outflow in the parsec-scale molecular torus of NGC 1068. *Astrophys. J. Lett.* **884**, L28 (2019).
27. Viti, S. et al. Molecular line emission in NGC 1068 imaged with ALMA. II. The chemistry of the dense molecular gas. *Astron. Astrophys.* **570**, A28 (2014).
28. Kelly, G. et al. Molecular shock tracers in NGC 1068: SiO and HNCO. *Astron. Astrophys.* **597**, A11 (2017).
29. Huang, K. Y. et al. The chemical footprint of AGN feedback in the outflowing circumnuclear disk of NGC 1068. *Astron. Astrophys.* **666**, A102 (2022).
30. Maiolino, R. et al. Evidence of strong quasar feedback in the early Universe. *Mon. Not. R. Astron. Soc.* **425**, L66–L70 (2012).
31. Lamastra, A. et al. Galactic outflow driven by the active nucleus and the origin of the gamma-ray emission in NGC 1068. *Astron. Astrophys.* **596**, A68 (2016).
32. Ramos Almeida, C. et al. The infrared nuclear emission of Seyfert galaxies on parsec scales: testing the clumpy torus models. *Astrophys. J.* **702**, 1127–1149 (2009).
33. Markowitz, A. G., Krumpe, M. & Nikutta, R. First X-ray-based statistical tests for clumpy-torus models: eclipse events from 230 years of monitoring of Seyfert AGN. *Mon. Not. R. Astron. Soc.* **439**, 1403–1458 (2014).
34. Marinucci, A. et al. NuSTAR catches the unveiling nucleus of NGC 1068. *Mon. Not. R. Astron. Soc.* **456**, L94–L98 (2016).
35. GRAVITY Collaboration. An image of the dust sublimation region in the nucleus of NGC 1068. *Astron. Astrophys.* **634**, A1 (2020).
36. Gámez Rosas, V. et al. Thermal imaging of dust hiding the black hole in NGC 1068. *Nature* **602**, 403–407 (2022).
37. Brandt, W. N. & Alexander, D. M. Cosmic X-ray surveys of distant active galaxies. The demographics, physics, and ecology of growing supermassive black holes. *Astron. Astrophys. Rev.* **23**, 1 (2015).
38. De Marco, B., Motta, S. E. & Belloni, T. M. in *Handbook of X-ray and Gamma-ray Astrophysics* (eds Bambi, C. & Santangelo, A.) 1–41 (Springer Nature Singapore, 2022).
39. Liang, E. P. T. On the hard X-ray emission mechanism of active galactic nuclei sources. *Astrophys. J. Lett.* **231**, L111–L114 (1979).
40. Alston, W., Giustini, M. & Petrucci, P.-O. in *Handbook of X-ray and Gamma-ray Astrophysics* (eds Bambi, C. & Santangelo, A.) 1–51 (Springer Nature Singapore, 2022).
41. Lasota, J.-P. AGN accretion discs. Preprint at https://arxiv.org/abs/2302.07925 (2023).
42. Gianolli, V. E. et al. Uncovering the geometry of the hot X-ray corona in the Seyfert galaxy NGC 4151 with IXPE. *Mon. Not. R. Astron. Soc.* **523**, 4468–4476 (2023).
43. Tagliacozzo, D. et al. The geometry of the hot corona in MCG-05-23-16 constrained by X-ray polarimetry. *Mon. Not. R. Astron. Soc.* **525**, 4735–4743 (2023).
44. Ingram, A. et al. The X-ray polarization of the Seyfert 1 galaxy IC 4329A. *Mon. Not. R. Astron. Soc.* **525**, 5437–5449 (2023).
45. Zaino, A. et al. Probing the circumnuclear absorbing medium of the buried AGN in NGC 1068 through NuSTAR observations. *Mon. Not. R. Astron. Soc.* **492**, 3872–3884 (2020).
46. Duras, F. et al. Universal bolometric corrections for active galactic nuclei over seven luminosity decades. *Astron. Astrophys.* **636**, A73 (2020).
47. Spinoglio, L., Fernández-Ontiveros, J. A. & Malkan, M. A. The high-ionization IR fine structure lines as bolometric indicators of the AGN power: study of the complete 12 μm AGN Sample. *Astrophys. J.* **941**, 46 (2022).
48. Abdo, A. A. et al. Fermi Large Area Telescope first source catalog. *Astrophys. J. Suppl. Ser.* **188**, 405–436 (2010).
49. Lenain, J. P., Ricci, C., Türler, M., Dorner, D. & Walter, R. Seyfert 2 galaxies in the GeV band: jets and starburst. *Astron. Astrophys.* **524**, A72 (2010).
50. Abdollahi, S. et al. Fermi Large Area Telescope fourth source catalog. *Astrophys. J. Suppl. Ser.* **247**, 33 (2020).
51. Aharonian, F. et al. Observations of selected AGN with HESS. *Astron. Astrophys.* **441**, 465–472 (2005).
52. Acciari, V. A. et al. Constraints on gamma-ray and neutrino emission from NGC 1068 with the MAGIC Telescopes. *Astrophys. J.* **883**, 135 (2019).
53. Albert, A. et al. A survey of active galaxies at TeV photon energies with the HAWC Gamma-Ray Observatory. *Astrophys. J.* **907**, 67 (2021).
54. Ajello, M., Di Mauro, M., Paliya, V. S. & Garrappa, S. The γ-ray emission of star-forming galaxies. *Astrophys. J.* **894**, 88 (2020).
55. Peretti, E., Blasi, P., Aharonian, F. & Morlino, G. Cosmic ray transport and radiative processes in nuclei of starburst galaxies. *Mon. Not. R. Astron. Soc.* **487**, 168–180 (2019).
56. Ajello, M., Murase, K. & McDaniel, A. Disentangling the hadronic components in NGC 1068. *Astrophys. J. Lett.* **954**, L49 (2023).
57. Ajello, M. et al. Gamma rays from fast black-hole winds. *Astrophys. J.* **921**, 144 (2021).
58. Fiore, F. et al. AGN wind scaling relations and the co-evolution of black holes and galaxies. *Astron. Astrophys.* **601**, A143 (2017).
59. Tombesi, F. et al. Evidence for ultra-fast outflows in radio-quiet AGNs. I. Detection and statistical incidence of Fe K-shell absorption lines. *Astron. Astrophys.* **521**, A57 (2010).
60. McDaniel, A., Ajello, M. & Karwin, C. Gamma-ray emission from galaxies hosting molecular outflows. *Astrophys. J.* **943**, 168 (2023).
61. Paiano, S. et al. The spectra of IceCube Neutrino (SIN) candidate sources – III. Optical spectroscopy and source characterization of the full sample. *Mon. Not. R. Astron. Soc.* **521**, 2270–2289 (2023).
62. Abbasi, R. et al. IceCube high-energy starting event sample: description and flux characterization with 7.5 years of data. *Phys. Rev. D* **104**, 022002 (2021).

63. Ballet, J., Burnett, T. H., Digel, S. W. & Lott, B. Fermi Large Area Telescope fourth source catalog data release 2. Preprint at https://arxiv.org/abs/2005.11208 (2020).
64. Abbasi, R. et al. first neutrino point-source results from the 22 string Icecube Detector. *Astrophys. J. Lett.* **701**, L47–L51 (2009).
65. Aartsen, M. G. et al. Time-integrated neutrino source searches with 10 years of IceCube data. *Phys. Rev. Lett.* **124**, 051103 (2020).
66. Berezinskii, V. S., Bulanov, S. V., Dogiel, V. A. & Ptuskin, V. S. *Astrophysics of Cosmic Rays* (ed. Ginzburg, V. L.) (Amsterdam: North-Holland, 1990).
67. Gaisser, T. K., Engel, R. & Resconi, E. *Cosmic Rays and Particle Physics* (Cambridge Univ. Press, 2016).
68. Mücke, A., Rachen, J. P., Engel, R., Protheroe, R. J. & Stanev, T. Photohadronic processes in astrophysical environments. *Publ. Astron. Soc. Aust.* **16**, 160–166 (1999).
69. Gould, R. J. & Schréder, G. P. Pair production in photon-photon collisions. *Phys. Rev.* **155**, 1404–1407 (1967).
70. Aharonian, F. A. *Very High Energy Cosmic Gamma Radiation: A Crucial Window on the Extreme Universe* (World Scientific, 2004).
71. Inoue, Y., Khangulyan, D., Inoue, S. & Doi, A. On high-energy particles in accretion disk coronae of supermassive black holes: implications for MeV gamma-rays and high-energy neutrinos from AGN cores. *Astrophys. J.* **880**, 40 (2019).
72. Caputo, R. et al. All-sky medium energy gamma-ray observatory eXplorer mission concept. *J. Astron. Telesc. Instrum. Syst.* **8**, 044003 (2022).
73. de Angelis, A. et al. Science with e-ASTROGAM. A space mission for MeV-GeV gamma-ray astrophysics. *J. High Energy Astrophys.* **19**, 1–106 (2018).
74. Gabici, S. & Aharonian, F. A. Gamma ray signatures of ultra high energy cosmic ray accelerators: electromagnetic cascade versus synchrotron radiation of secondary electrons. *Astrophys. Space Sci.* **309**, 465–469 (2007).
75. Murase, K. Hidden hearts of neutrino active galaxies. *Astrophys. J. Lett.* **941**, L17 (2022).
76. Berezinsky, V. S. in *Proc. International Conference Neutrino '77* (eds Faissner, H. et al.) 650 (Friedrich Vieweg & Sohn Verlagsgesellschaft mbH, Braunschweig, 1977).
77. Eichler, D. High-energy neutrino astronomy: a probe of galactic nuclei? *Astrophys. J.* **232**, 106–112 (1979).
78. Silberberg, R. & Shapiro, M. M. Neutrinos as a probe for the nature of and processes in active galactic nuclei. In *Proc. 16th International Cosmic Ray Conference* Vol. 10 (ed. Miyake, S.) 357 (Institute for Cosmic Ray Research, 1979).
79. Inoue, Y., Khangulyan, D. & Doi, A. On the origin of high-energy neutrinos from NGC 1068: the role of nonthermal coronal activity. *Astrophys. J. Lett.* **891**, L33 (2020).
80. Murase, K., Kimura, S. S. & Mészáros, P. Hidden cores of active galactic nuclei as the origin of medium-energy neutrinos: critical tests with the MeV gamma-ray connection. *Phys. Rev. Lett.* **125**, 011101 (2020).
81. Yoast-Hull, T. M., Gallagher I, J. S., Zweibel, E. G. & Everett, J. E. Active galactic nuclei, neutrinos, and interacting cosmic rays in NGC 253 and NGC 1068. *Astrophys. J.* **780**, 137 (2014).
82. Eichmann, B., Oikonomou, F., Salvatore, S., Dettmar, R.-J. & Tjus, J. B. Solving the multimessenger puzzle of the AGN-starburst composite galaxy NGC 1068. *Astrophys. J.* **939**, 43 (2022).
83. Peretti, E. et al. Diffusive shock acceleration at EeV and associated multimessenger flux from ultra-fast outflows driven by active galactic nuclei. *Mon. Not. R. Astron. Soc.* **526**, 181–192 (2023).
84. Inoue, S., Cerruti, M., Murase, K. & Liu, R.-Y. High-energy neutrinos and gamma rays from winds and tori in active galactic nuclei. Preprint at https://arxiv.org/abs/2207.02097 (2022).
85. Salvatore, S., Eichmann, B., Rodrigues, X., Dettmar, R. J. & Becker Tjus, J. On the possible jet contribution to the γ-ray luminosity in NGC 1068. *Astron. Astrophys.* **687**, A139 (2024).
86. Fang, K., Lopez Rodriguez, E., Halzen, F. & Gallagher, J. S. High-energy neutrinos from the inner circumnuclear region of NGC 1068. *Astrophys. J.* **956**, 8 (2023).
87. Michiyama, T., Inoue, Y., Doi, A. & Dmitry, K. ALMA detection of parsec-scale blobs at the head of a kiloparsec-scale jet in the nearby Seyfert galaxy NGC 1068. *Astrophys. J. Lett.* **936**, L1 (2022).
88. Ghisellini, G., Haardt, F. & Fabian, A. C. On re-acceleration, pairs and the high-energy spectrum of AGN and galactic black hole candidates. *Mon. Not. R. Astron. Soc.* **263**, L9–L12 (1993).
89. Fabian, A. C. et al. Properties of AGN coronae in the NuSTAR era. *Mon. Not. R. Astron. Soc.* **451**, 4375–4383 (2015).
90. Fabian, A. C., Lohfink, A., Belmont, R., Malzac, J. & Coppi, P. Properties of AGN coronae in the NuSTAR era - II. Hybrid plasma. *Mon. Not. R. Astron. Soc.* **467**, 2566–2570 (2017).
91. Olivares, H. R., Mościbrodzka, M. A. & Porth, O. General relativistic hydrodynamic simulations of perturbed transonic accretion. *Astron. Astrophys.* **678**, A141 (2023).
92. Jiang, Y.-F., Blaes, O., Stone, J. M. & Davis, S. W. Global radiation magnetohydrodynamic simulations of sub-Eddington accretion disks around supermassive black holes. *Astrophys. J.* **885**, 144 (2019).
93. Fiorillo, D. F. G., Petropoulou, M., Comisso, L., Peretti, E. & Sironi, L. TeV neutrinos and hard X-rays from relativistic reconnection in the corona of NGC 1068. *Astrophys. J. Lett.* **961**, L14 (2024).
94. Mbarek, R., Philippov, A., Chernoglazov, A., Levinson, A. & Mushotzky, R. Interplay between accelerated protons, x-rays and neutrinos in the corona of NGC 1068: constraints from kinetic plasma simulations. *Phys. Rev. D* **109**, L101306 (2024).
95. Abbasi, R. et al. Extending the IceCube search for neutrino point sources in the northern sky with additional years of data. In *Proc. 38th International Cosmic Ray Conference* 1060 (Proceedings of Science, 2023).
96. Kheirandish, A., Murase, K. & Kimura, S. S. High-energy neutrinos from magnetized coronae of active galactic nuclei and prospects for identification of Seyfert galaxies and quasars in neutrino telescopes. *Astrophys. J.* **922**, 45 (2021).
97. Ricci, C. et al. BAT AGN spectroscopic survey. V. X-ray properties of the Swift/BAT 70-month AGN catalog. *Astrophys. J. Suppl. Ser.* **233**, 17 (2017).
98. Abbasi, R. et al. Searching for high-energy neutrino emission from Seyfert galaxies in the northern sky with IceCube. In *Proc. 38th International Cosmic Ray Conference* 1052 (Proceedings of Science, 2023).
99. Abbasi, R. et al. Search for TeV neutrinos from Seyfert galaxies in the southern sky using starting track events in IceCube. In *Proc. 38th International Cosmic Ray Conference* 1533 (Proceedings of Science, 2023).
100. Abbasi, R. et al. Search for high-energy neutrino emission from hard X-ray AGN with IceCube. In *Proc. 38th International Cosmic Ray Conference* 1032 (Proceedings of Science, 2023).
101. Tanimoto, A., Ueda, Y., Odaka, H., Yamada, S. & Ricci, C. NuSTAR Observations of 52 Compton-thick active galactic nuclei selected by the Swift/Burst Alert Telescope all-sky hard X-ray survey. *Astrophys. J. Suppl. Ser.* **260**, 30 (2022).
102. Neronov, A., Savchenko, D. & Semikoz, D. V. Neutrino signal from a population of Seyfert galaxies. *Phys. Rev. Lett.* **132**, 101002 (2024).
103. Padovani, P. et al. Dissecting the region around IceCube-170922A: the blazar TXS 0506+056 as the first cosmic neutrino source. *Mon. Not. R. Astron. Soc.* **480**, 192–203 (2018).
104. Murase, K., Guetta, D. & Ahlers, M. Hidden cosmic-ray accelerators as an origin of TeV-PeV cosmic neutrinos. *Phys. Rev. Lett.* **116**, 071101 (2016).

Acknowledgements
The idea for this Review came during a Topical Workshop on NGC 1068 organized by E.R., C.B. and P.P. and held at the Munich Institute for Astro-, Particle and BioPhysics in Garching on 6–10 March 2023. As the organizers and invited speakers, we wish to thank all of the participants in the meeting for the stimulating atmosphere and fruitful discussions. This work is supported by the Deutsche Forschungsgemeinschaft (DFG, German Research Foundation) through grant number SFB 1258 'Neutrinos and Dark Matter in Astro- and Particle Physics' and by the Excellence Cluster ORIGINS, which is funded by the DFG under Germany's Excellence Strategy EXC 2094. B.E. acknowledges support from the DFG within the Collaborative Research Center grant number SFB 1491 'Cosmic Interacting Matters – From Source to Signal'. E.P. acknowledges support from the Villum Fonden (grant number 18994) and from the European Union's Horizon 2020 research and innovation programme under the Marie Sklodowska-Curie grant agreement number 847523 'INTERACTIONS'. S.G. and E.P. were also supported by Agence Nationale de la Recherche (grant number ANR-21-CE31-0028).

Author contributions
P.P. coordinated the work, contributing mostly to the 'Main', the 'Multi-messenger view', the 'Relevant powers and the case for a 'hidden' source scenario' and the 'Conclusions' sections and the Supplementary Information, and collaborated with E.R. on finalizing the paper. E.R. also contributed to the 'Main' and 'Conclusions' sections. K.-Y.H. worked on the 'Sub-millimetre band and molecular outflow power' section, while V.G.R. and T.S. focused on the 'Near-IR band and the torus' section, S.B. on the 'X-ray band and AGN power' section, M.A. and A.L. on the 'Gamma-ray band and SB power' section, C.B. on 'Teraelectronvolt neutrino band' and 'Outlook' sections, S.G. on the 'Relevant powers and the case for a 'hidden' source scenario' section, E.P., B.E., D.G. and A.L. on the 'Nailing down the hidden source case' section, P.B. on the 'Nailing down the hidden source case' section and the Supplementary Information, and H.N. on the 'Outlook' section. All authors participated in discussions regarding the manuscript.

Competing interests
The authors declare no competing interests.

Additional information
Supplementary information The online version contains supplementary material available at https://doi.org/10.1038/s41550-024-02339-z.

Correspondence and requests for materials should be addressed to P. Padovani.

Peer review information *Nature Astronomy* thanks the anonymous reviewers for their contribution to the peer review of this work.